Surfaces Affect Ion Pairing

Ilya Chorny, Ken A. Dill,*,† and Matthew P. Jacobson*,‡

Department of Pharmaceutical Chemistry, University of California, San Francisco, California 94143-2240

Received: September 6, 2005

In water, positive ions attract negative ions. That attraction can be modulated if a hydrophobic surface is present near the two ions in water. Using computer simulations with explicit and implicit water, we study how an ion embedded on a hydrophobic surface interacts with another nearby ion in water. Using hydrophobic surfaces with different curvatures, we find that the contact interaction between a positive and negative ion is strongly affected by the curvature of an adjacent surface, either stabilizing or destabilizing the ion pair. We also find that the solvent-separated ion pair (SSIP) can be made more stable than the contacting ion pair by the presence of a surface. This may account for why bridging waters are often found in protein crystal structures. We also note that implicit solvent models do not account for SSIPs. Finally, we find that there are charge asymmetries: an embedded positive charge attracting a negative ion is different than an embedded negative charge attracting a positive ion. Such asymmetries are also not predicted by implicit solvent models. These results may be useful for improving computational models of solvation in biology and chemistry.

Introduction

Ionic charges of opposite sign often pair together to form salt bridges: within protein structures, between ligands and proteins, and at membrane surfaces, as well as in nonbiological systems. To predict the stabilities, binding affinities, and kinetics of formation of such systems, it is necessary to be able to predict the interaction free energies of ion pairs. Ion pairing has been studied by computer simulations utilizing either explicit solvent models or implicit Poisson−Boltzmann or Generalized Born models. Though a few studies have considered the effects of the macromolecular environment on the strengths of salt bridges,[1−6] most studies so far have considered only two isolated ions in water. Our interest here is in understanding how the presence of a surface in the vicinity can affect the interaction free energies of ions in water. We examine how the effect of the surface varies with its curvature, from concave to planar to convex. Other studies have considered hydration of model systems[7] and macromolecular surfaces with varying curvature[8−10] but have not explicitly examined the strengths of ion pairs.

The attraction of a positive ion for a negative ion in water can drive the two ions to come into contact, called the contact ion pair (CIP) state. For typical monatomic ions [11] and ionizable amino acid side-chain analogues,[12] the CIP state is the most stable state in solution. However, it is often observed in studies of potentials of mean force (PMF) that a second type of state can also be quite stable. The solvent-separated ion pair (SSIP) is a state in which two ions are separated by a water molecule.[12−14] Yu et al.[15] found that there exist a significant number of solvent-separated salt bridges in crystal structures of proteins. A limitation of current implicit solvent models is that they treat water as a continuum and thus are not able to capture features of solvation such as SSIPs. In the present work, we explore PMFs of ions in water and near surfaces, and we compare explicit and implicit water models.

Methods

To model a hydrophobic surface of a given curvature, we create in the computer a molecular wall that is assembled from Lennard−Jones (LJ) spheres. Figure 1 shows the surfaces: one is planar, three have negative curvature (representing surfaces of rodlike structures; we call these "bumpers"), and three have positive curvature (representing cylindrical cavities; we call these "receptors"). The radii of curvature are 6, 9, or 12 Å for both positively and negatively curved surfaces. The surfaces and ions are fully surrounded by water. One ion is embedded within the first layer of the wall (the embedded ion), and the other (the solute ion) is free to move along an axis normal to the surface, away from the embedded ion. In addition to its charge, the solute ion is also a LJ sphere, with otherwise the same size and energetic parameters as the spheres that are used to construct the surfaces. The method of building surfaces from individual LJ spheres is similar in spirit to previous work done by Choudhury and Pettitt.[16] The LJ parameters are chosen to be identical to those of a single united atom methane molecule in the Gromos 96 force field ($\sigma = 3.71$ Å, $\epsilon = 0.3$ kcal/mol). Each hydrophobic wall is three layers thick. Each wall has one 7×7 layer of LJ spheres, shown in yellow, and two fill layers, shown in green. The fill layers contain a different number of LJ spheres, depending on the curvature of the surface. The embedded ion is a single point charge on the sphere shown in black on the figure.

For each hydrophobic wall, we performed three simulations: (1) explicit solvent with a positive embedded charge and a negative solute charge, (2) explicit solvent with a negative embedded charge and a positive solute charge, and (3) one Poisson−Boltzmann implicit-solvent simulation. Implicit solvent models do not depend on the relative signs of embedded and solute charges, so only one simulation is needed for this case. As a reference simulation, we also computed the PMF of the two ions in water, in the absence of a surface.

* Authors to whom correspondence should be addressed.
† Telephone: 415-476-9964. Fax: 415-502-4222. E-mail: dill@maxwell.ucsf.edu.
‡ Telephone: 415-514-9811. Fax: 415-514-4260. E-mail: matt@cgl.ucsf.edu.

10.1021/jp055043m CCC: $30.25
Published on Web 11/30/2005

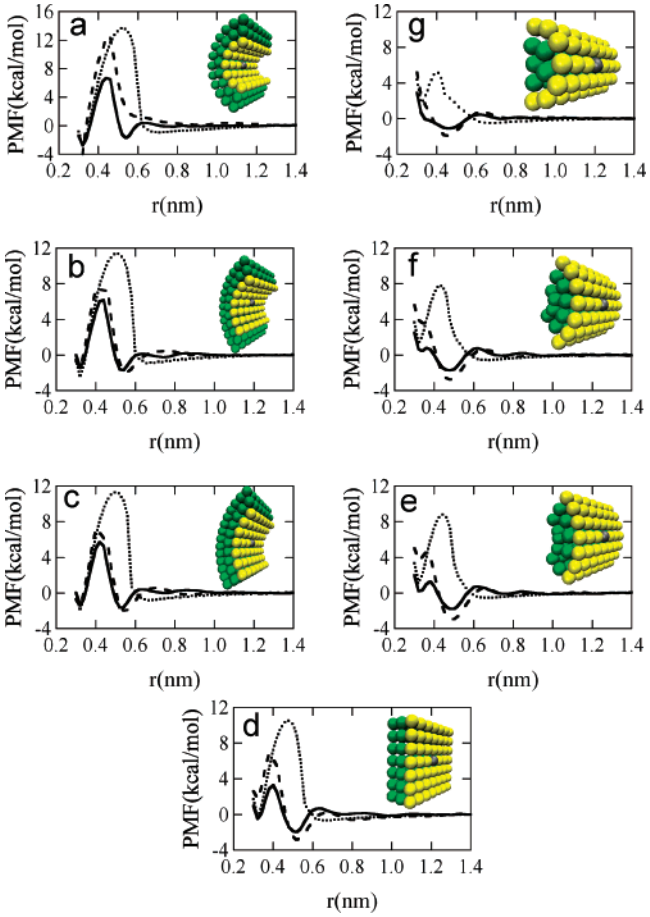

Figure 1. Potentials of mean force between a free solute ion in water and an embedded ion of opposite charge on a surface. The black ball indicates the position of the embedded charge. Solid line: positive surface, negative solute, explicit solvent. Dashed line: negative surface, positive solute, explicit solvent. Dotted line: FDPB implicit solvent calculation. Radii of curvature: 6 Å for surfaces a (concave) and g (convex), 9 Å for surfaces b (concave) and f (convex), and 12 Å for surfaces c (concave) and e (convex). Surface d is a plane.

Molecular dynamics simulations were performed using the Gromacs 3.2.1 program.[17−19] The surface and solute were embedded in roughly 2000 SPC[20] water molecules in an equilibrated cubic simulation box with periodic boundary conditions. The temperature was kept constant at 298 K using the Nose−Hoover[21,22] thermostat with a relaxation time of 0.1 ps. The pressure was kept constant at 1 atm by applying the Berendsen[23] weak-coupling algorithm with a relaxation time of 0.5 ps and an isothermal compressibility of 4.5×10^{-5} (kJ mol^{-1} nm^{-3}). The long-range electrostatics were accounted for using Particle-Mesh Ewald summation (PME)[24,25] with a real-space cutoff of 9 Å for the nonbonded interaction. The integration time step was 2 fs, and the pair list was updated every 20 fs. A velocity version of the Verlet algorithm[26,27] was used to propagate the system in time.

We calculated the PMF values using umbrella sampling. The distance between the solute and the reference sphere is constrained to a narrow linear range of the reaction coordinate normal to the reference sphere, using a quadratic biasing potential,

$$V(r) = k(r - r_i)^2$$

where k (6000 kJ/nm^2) is the biasing force constant and r_i is the point about which the distances are constrained. The distribution of the distances, $P(r_i)$, for each window is then used to calculate the free energy as a function of the distance between the solute and the reference sphere using the expression

$$\Delta G(r) = -k_B T \ln[P_i(r)] + C_i$$

where k_B is the Boltzmann constant and C_i is the free energy between neighboring windows.

We used 23 windows between 3 and 14 Å, centered at 0.5-Å intervals. The resulting $P(r_i)$ is then processed using the weighted histogram analysis method,[28,29] where the individual $P(r_i)$ data are combined into a single $P(r)$ curve so as to minimize the statistical error in the total probability distribution. The resulting PMFs were shifted vertically to set the average value of the free energy at a separation distance between 12 and 14 Å to zero.

In addition to explicit-water simulations, we also treated each ion-pair-plus-surface system with implicit solvent calculations using the Finite Difference Poisson−Boltzmann (FDPB) method implemented in the program Delphi.[30,31] We set the solvent dielectric constant to 80 and used a lattice spacing of 5 grids/Å. We chose a lattice dimension to ensure that a cube the size of the largest x, y, or z dimension filled 85% of the lattice (reducing this percentage to 50% made no significant difference in the results). The interaction between the solute and the surface was treated using the same potential energy function as in the molecular dynamics calculation. The FDPB solvation free energy was calculated using three different radii for the spheres: the LJ radius of 1.9 Å, a radius that is 8% larger (2.055Å), and a radius that is 5% smaller (1.8 Å). The three different radii were used because PB methods frequently treat the atomic radius as an adjustable parameter, to better reproduce experimental measurements. The value of 2.055 Å was chosen as the default value because it best reproduced the value of the CIP state for surface A in Figure 1.

We accounted for the nonpolar contribution to the solvation free energy using a solvent-accessible surface-area (SASA)-based term, with a proportionality constant $\gamma = 0.009$ kcal/Å^2. Solvent-accessible surface areas were calculated using the MSMS program[32] based on the same atomic radii as in the FDPB calculation. The solvation free energy as a function of the distance between the solute and the reference sphere was calculated in a manner analogous to the molecular dynamics simulations described above. We generated 23 configurations in which the distance between the solute and the reference sphere ranged between 3 and 14 Å, spaced 0.5 Å apart, and determined their corresponding solvation free energies. The resulting PMF was then calculated using the expression

$$\Delta G(r) = V(r) + \Delta G_{PB}(r) + \gamma \mathrm{SASA}(r)$$

where $V(r)$ is the interaction potential between the solute and the surface, $\Delta G_{PB}(r)$ is the solvation free energy obtained from the FDPB method, and SASA(r) is the solvent-accessible surface area as a function of the distance between the solute and the surface. We note that SASA changes only when the distance between the solute and the reference sphere is less than about 6 Å. As previously described, the resulting PMFs are shifted vertically such that the average value of the PMF between 12 and 14 Å is zero.

Results

(1) The Strength of an Ion Pair Depends on the Curvature of the Adjacent Surface. As expected, our reference calculations show that the most stable configuration of a positive and

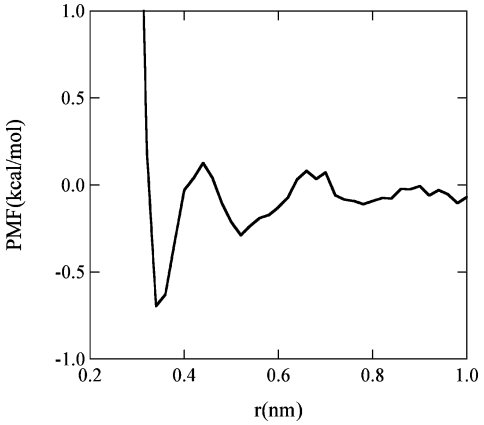

Figure 2. PMF for a positive and negative ion in bulk water.

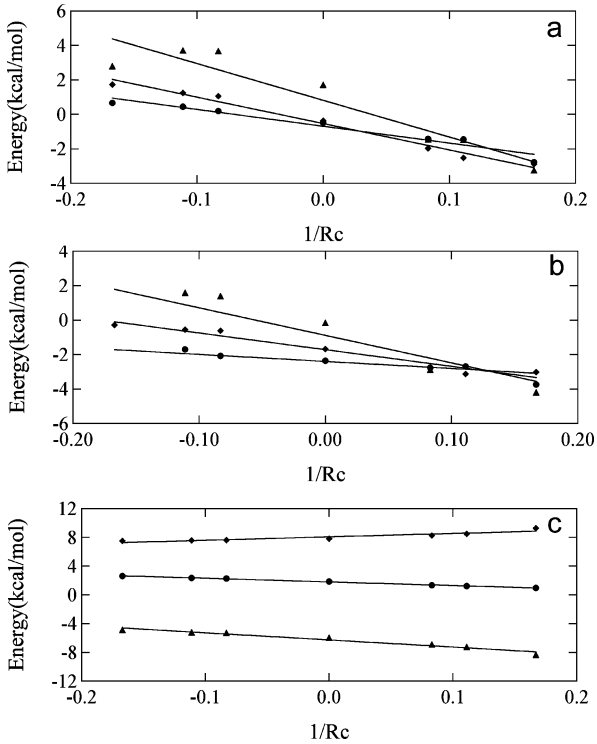

Figure 3. Free energy vs inverse radius of curvature of the surface for the CIP state: (a) the total free energy, (b) the solvent component of the free energy, (c) the LJ component (between the solute and the surface) of the solute free energy. In panels a and b, the circles are for a positive surface and a negative solute, the triangles are for a negative surface and a positive solute, and the diamonds are for the implicit water simulation. In panel c, the circles are for the overall LJ component, the triangles are for the attractive part of the LJ potential ($1/r^6$), and the diamonds are for the repulsive part ($1/r^{12}$).

negative ion in water, in the absence of a surface, is the CIP state (see Figure 2). More surprisingly, we find that the stability of the CIP state is strongly affected by the curvature of the adjacent hydrophobic surface (see Figure 1). There is some precedent for curvature dependence of solvation effects. In particular, Wallqvist and Berne demonstrated that the solvation free energy of a hydrophobic particle is curvature-dependent.[7] Here we observe that receptor surfaces (positively curved) stabilize the ion-pair contact state whereas bumper surfaces (negatively curved) destabilize the CIP state.

Figure 3 shows that this curvature dependence can be made approximately linear by plotting the relative free energy of the CIP versus the inverse of the radius of the surface curvature. The effects of curvature are most pronounced for the surface with the negatively charged embedded ion, and they are least pronounced for the surface with the positive embedded ion. Poisson−Boltzmann predicts a curvature dependence in the right range, but does not predict the charge asymmetry. Also, whereas PB predicts that ion pairs in contact are stable (i.e., represent a local minimum on the PMF) for all surfaces, the explicit-solvent simulations show that ion pairs do not form stable contacts at strongly curved bumper surfaces.

What is the physical basis for the curvature effects? Figure 3 shows the breakdown in terms of free energy components. As surface curvature becomes more negative (from bumpers to planes to receptors), the surface increasingly stabilizes the ion pair. This comes about for two reasons. First, with increasingly positive curvature, the solute ion in contact with the surface has increasingly favorable Lennard−Jones interactions with the surface because receptor surfaces have more atoms close to the solute ion than bumper surfaces have. Second, the presence of a surface also enhances the electrostatic interactions, in a way that is captured in the PB model. A simple way to see this is through the concept of image charge. An ion in water near a low-dielectric surface will see an image of itself, as if it were looking in a mirror, leading to a repulsion from the surface. Since the embedded ion generates a stronger image than the solute ion (since it is closer), the solute ion "sees" not just the embedded ion but also the image of the embedded ion, so it has nearly double the attraction to the embedded ion. This image electrostatics effect (a) tends to stabilize an ion pair, and (b) depends on curvature because the position of the image behind the plane shifts toward the water interface for receptors and away from the interface for bumpers.

A key implication of these results is that to predict the affinity of a charged ligand for a charge inside a protein receptor site, you need to know the curvature of the receptor site. These effects can be large: a few kcal/mol. Such curvature effects are not usually taken into account in simple models of binding affinity.

(2) The Most Stable State Is Often the Solvent-Separated Ion Pair. Computer simulations of oppositely charged ions in explicit water typically indicate that the most stable state occurs when the two ions come into contact. Implicit models, too, predict that ions come into contact in water. However, our simulations show that the presence of a nearby surface can cause the solvent-separated state to become more stable than the contact state. A comparison of both free energy minima (CIP vs SSIP) in the panels in Figure 1 shows that the only two situations in which the CIP state is preferred to the SSIP state are (1) inside tightly curved receptors, and (2) for isolated ions (Figure 2). Near bumpers and planes and weakly curved receptors, the SSIP is more stable than the CIP. This may account for the observation of Yu et al. that ion pairs are commonly found separated by a bridging water in protein crystal structures.[15] Although Masunov and Lazaridis[12] found amino acid side-chain analogues to prefer the CIP state, they did not consider the effects of neighboring surfaces.

It is worth noting a difference between our wall simulations versus our isolated ions in water. In the bulk, a factor of $4\pi r^2$ is usually incorporated into the PMF for averaging due to the spherical symmetry. However, in the presence of a wall, there is no such corresponding symmetry, so we do not include that factor in those cases.

(3) Charge Asymmetry: A Positive Surface Is Different than a Negative Surface. Figure 1 shows that a positively charged solute near a negative embedded charge is different than a negatively charged solute near a positive embedded

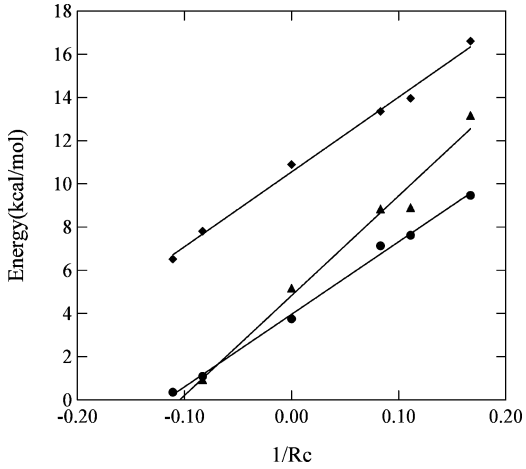

Figure 4. The free energy barrier from the CIP to SSIP state vs inverse radius of curvature of the surface. Circles are for a positive surface and a negative solute in explicit water, triangles are for a negative surface and a positive solute in explicit water, and the diamonds are for the implicit water simulation.

charge. Implicit solvent models would predict no difference. We find the largest charge asymmetries for bumper surfaces and smallest for receptor surfaces. This asymmetry is a consequence of the way in which a charge structures the surrounding water molecules. When solvating a positive charge a water molecule will point its negative dipole toward the charge, whereas when solvating a negative charge it will point one of its OH bonds toward a negative charge.[33] As a result we find that the potential energy between a negative ion and the surrounding water (−87 kcal/mol) is about three times greater than the potential energy between a positive ion and the surrounding water (−25 kcal/mol). This effect is not captured by FDPB, which treats water as a dielectric continuum, and neglects its molecular structure.

(4) PB Overestimates the Barriers to Ion Dissociation. Figure 4 shows the heights of the free energy barriers for moving an ion from contact (the CIP state) to solvent-separated (the SSIP state). The figure shows a large dependence on the wall curvature. A solute ion encounters a bigger barrier to enter a receptor than to contact a bumper, and the difference in barrier height can be as large as 8 kcal/mol. The PB model captures this trend, but systematically overestimates the barrier by about 4−6 kcal/mol.

Can we repair the PB overestimation of the barrier height by adjusting the charge radii? To test this, we decreased the radius of the spheres from the default FDPB radius (2.055 Å) to the LJ radius (1.9 Å) used in the explicit water simulations. In short, Figure 5 shows that if we adjust the charge radii to force the PB model to produce barrier heights in agreement with the explicit-solvent simulations, then it spoils the agreement of the CIP stabilities. Figure 6 shows that the PB model also overestimates the barrier width.

In the FDPB simulation, the barrier results from the method by which the dielectric surface is calculated. At a critical distance, where the ions are roughly one probe distance apart (∼1.4 Å), the two surfaces (surface and solute), as measured by the probe, merge and the dielectric between the surface and the solute is low. Beyond this distance, the dielectric constant between the two ions is treated as high dielectric. While the two surfaces are merged, the increase in the amount of low dielectric, as the solute is moved away from the surface, in the high dielectric medium causes an increase in the solvation free energy of the ions, resulting in a separation barrier.

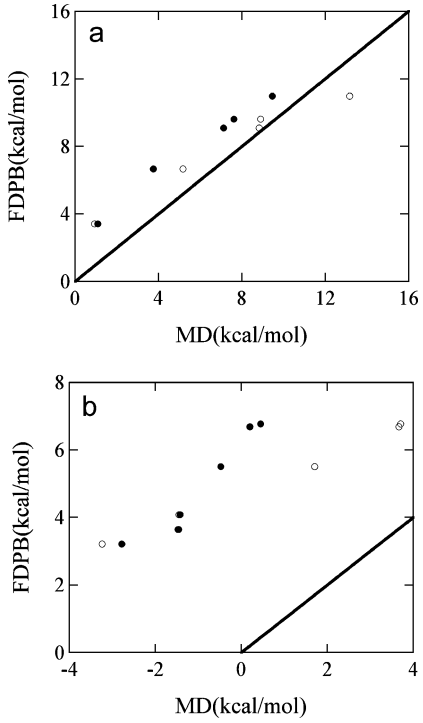

Figure 5. Correlation between explicit water and FDPB simulations, of the relative stabilities of (a) barrier heights, and (b) the CIP state, using the LJ radius (1.9 Å) for the spheres. The solid circles are for a positive surface and a negative solute, and the open circles are for a negative surface and a positive solute. The solid line is $y = x$, the perfect correlation reference.

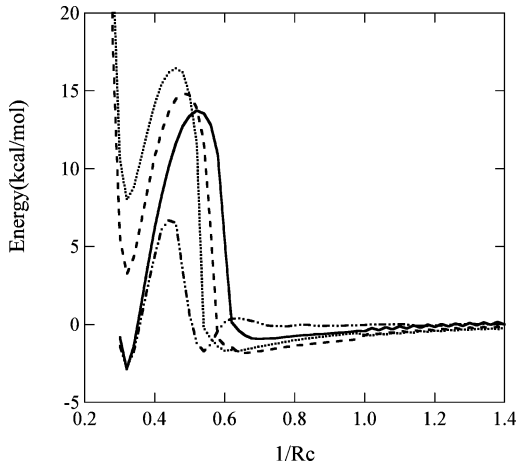

Figure 6. PMFs for the planar surface. The solid, dashed, and dotted lines are for FDPB using a sphere radius of 2.055, 1.9, and 1.8 Å, respectively. The dashed−dotted line is the PMF calculated using explicit water.

The barrier height can be attributed to two factors. First, in general, for potentials of mean force for most liquids, sufficiently small increases in separation beyond the contact separation opens up a vacuum between the molecules that is too small to be filled by solvent. This is energetically costly. This component of free energy arises from both implicit (as described above) and explicit models. A second contributor to the free energy barrier, which is not present in the implicit solvent models, arises because the solvent is water, which can form both hydrogen bonds with neighboring water molecules and polar bonds with the ions. We speculate that separation of the ions from the contact distance causes breaking of the hydrogen bond networks in the barrier region, resulting in a positive change in free

energy. As noted above, the dipole of water is asymmetrical, resulting in a barrier height that depends on the sign of the surface charge as shown in Figure 1.

Summary

We have used computer simulations to study the pairing of a positive and a negative ion in the vicinity of a hydrophobic surface. One ion is embedded in the surface, and the other is free in water adjacent to the surface. We consider surfaces of different shapes, from "receptors" (having negative curvature), to planes, to "bumpers" (having positive curvature). We find that ion-pairing free energies are affected significantly—including even their signs—by the presence and curvatures of the neighboring surfaces. We find that a solute ion is most stable in contact with an embedded charge in a receptor, but it will have a large entrance barrier. In contrast, a solute ion will not form a contact with an embedded charge on a bumper surface, but rather will form a stable solvent-separated ion pair instead. This may account for why protein structures so often include ion pairs that are separated by a single water molecule. Our results also have important implications for predicting electrostatic contributions to binding of polar/charged ligands in macromolecular cavities. We find charge asymmetries in the explicit solvent simulations that are not accounted for by implicit solvent models such as Poisson−Boltzmann.

Acknowledgment. We thank the NIH and Pfizer for support to K.D. and the Alfred P. Sloan Foundation for a postdoctoral fellowship to I.C. M.P.J. was supported by NSF Grant MCB-0346399, NIH Grant GM071790, and startup funds provided by HHMI Biomedical Research Support Program Grant No. 5300246 to the UCSF School of Medicine.

References and Notes

(1) Honig, B.; Hubbell, W. *Biophys. J.* **1983**, *41*, A203.
(2) Honig, B. H.; Hubbell, W. L. *Proc. Natl. Acad. Sci. U.S.A.*—Biol. Sci. **1984**, *81*, 5412.
(3) Sheinerman, F. B.; Honig, B. *J. Mol. Biol.* **2002**, *318*, 161.
(4) Sheinerman, F. B.; Norel, R.; Honig, B. *Curr. Opin. Struct. Biol.* **2000**, *10*, 153.
(5) Hendsch, Z. S.; Tidor, B. *Protein Sci.* **1994**, *3*, 211.
(6) Luo, R.; David, L.; Hung, H.; Devaney, J.; Gilson, M. K. *J. Phys. Chem. B* **1999**, *103*, 727.
(7) Wallqvist, A.; Berne, B. J. *J. Phys. Chem.* **1995**, *99*, 2885.
(8) Makarov, V.; Pettitt, B. M.; Feig, M. *Acc. Chem. Res.* **2002**, *35*, 376.
(9) Carey, C.; Cheng, Y. K.; Rossky, P. J. *Chem. Phys.* **2000**, *258*, 415.
(10) Cheng, Y. K.; Rossky, P. J. *Nature* **1998**, *392*, 696.
(11) Dang, L. X.; Rice, J. E.; Kollman, P. A. *J. Chem. Phys.* **1990**, *93*, 7528.
(12) Masunov, A.; Lazaridis, T. *J. Am. Chem. Soc.* **2003**, *125*, 1722.
(13) Kang, N. S.; Jung, D. H.; No, K. T.; Jhon, M. S. *Chem. Phys. Lett.* **2002**, *364*, 580.
(14) Rozanska, X.; Chipot, C. *J. Chem. Phys.* **2000**, *112*, 9691.
(15) Yu, Z. Y.; Jacobson, M. P.; Josovitz, J.; Rapp, C. S.; Friesner, R. A. *J. Phys.Chem.* B **2004**, *108*, 6643.
(16) Choudhury, N.; Pettitt, B. M. *J. Am. Chem. Soc.* **2005**, *127*, 3556.
(17) Berendsen, H. J. C.; Vanderspoel, D.; Vandrunen, R. *Comput. Phys. Commun.* **1995**, *91*, 43.
(18) Lindahl, E.; Hess, B.; van der Spoel, D. *J. Mol. Model.* **2001**, *7*, 306.
(19) Vandrunen, R.; Vanderspoel, D.; Berendsen, H. J. C. *Abstracts of Papers of the American Chemical Society* **1995**, *209*, 49.
(20) Berendsen, H. J. C.; Postma, J. P. M.; van Gunsteren, W. F.; Hermans, J. *Interaction Models for* Water *in Relation to Protein Hydration*.; In Intermolecular Forces; Pullman B, Ed.; D. Reidel: Dordrecht, The Netherlands, 1981.
(21) Hoover, W. G. *Phys. Rev. A* **1985**, *31*, 1695.
(22) Nose, S. *Mol. Phys.* **1984**, *52*, 255.
(23) Berendsen, H. J. C.; Postma, J. P. M.; Vangunsteren, W. F.; Dinola, A.; Haak, J. R. *J Chem. Phys.* **1984**, *81*, 3684.
(24) Darden, T.; York, D.; Pedersen, L. *J. Chem. Phys.* **1993**, *98*, 10089.
(25) Essmann, U.; Perera, L.; Berkowitz, M. L.; Darden, T.; Lee, H.; Pedersen, L. G. *J. Chem. Phys.* **1995**, *103*, 8577.
(26) Swope, W. C.; Andersen, H. C.; Berens, P. H.; Wilson, K. R. *J. Chem. Phys.* **1982**, *76*, 637.
(27) Verlet, L. *Phys. Rev.* **1967**, *159*, 98.
(28) Kumar, S.; Bouzida, D.; Swendsen, R. H.; Kollman, P. A.; Rosenberg, J. M. *J Comput. Chem.* **1992**, *13*, 1011.
(29) Souaille, M.; Roux, B. *Comput.r Phys. Commun.* **2001**, *135*, 40.
(30) Gilson, M. K.; Sharp, K.; Honig, B.; Fine, R.; Hagstrom, R. *Biophys. J.* **1987**, *51*, A234.
(31) Nicholls, A.; Honig, B. *J. Computat. Chem.* **1991**, *12*, 435.
(32) Sanner, M. F.; Olson, A. J.; Spehner, J. C. *Biopolymers* **1996**, *38*, 305.
(33) Hribar, B.; Southall, N. T.; Vlachy, V.; Dill, K. A. *J. Am. Chem. Soc.* **2002**, *124*, 12302.